Author's personal copy

Nuclear Instruments and Methods in Physics Research B 269 (2011) 3067–3073

Contents lists available at ScienceDirect

Nuclear Instruments and Methods in Physics Research B

journal homepage: www.elsevier.com/locate/nimb

Thorium partitioning in Greek industrial bauxite investigated by synchrotron radiation and laser-ablation techniques

P. Gamaletsos [a], A. Godelitsas [a,*], T.J. Mertzimekis [b], J. Göttlicher [c], R. Steininger [c], S. Xanthos [d], J. Berndt [e], S. Klemme [e], A. Kuzmin [f], G. Bárdossy [g]

[a] Faculty of Geology & Geoenvironment, University of Athens, Panepistimioupolis, 15784 Zographou, Greece
[b] Department of Physics, University of Athens, Panepistimioupolis, 15771 Zographou, Greece
[c] Karlsruhe Institute of Technology, Institute for Synchrotron Radiation, Hermann-von-Helmholtz-Platz 1, 76344 Eggenstein-Leopoldshafen, Germany
[d] Department of Electrical and Computer Engineering, Aristotle University of Thessaloniki, GR-54124 Thessaloniki, Greece
[e] Institut für Mineralogie, Corrensstrasse 24, Universität Münster, 48149 Münster, Germany
[f] Institute of Solid State Physics, University of Latvia, Kengaraga st. 8, 1063 Riga, Latvia
[g] Hungarian Academy of Sciences, H-1051 Budapest, Hungary

ARTICLE INFO

Article history:
Available online 22 April 2011

Keywords:
Bauxite
Aluminium
Thorium
Titanium oxides
Synchrotron
Micro-XRF spectroscopy
Micro-XAFS spectroscopy
Laser Ablation ICP-MS
Gamma-ray spectroscopy

ABSTRACT

Typical red–brown (Fe-rich) and high-quality white–grey (Fe-depleted) bauxite samples from active mines of the Parnassos-Ghiona area, central Greece, were investigated. According to XRF and ICP-MS analyses their actinide content, and particularly of Th, is relatively increased. Fe-depleted samples contain up to 62.75 ppm Th corresponding to 220 Bq/kg due to ^{228}Ac (^{232}Th-series), whereas Fe-rich samples are less Th-radioactive (up to 58.25 ppm Th, 180 Bq/kg due to ^{228}Ac). Powder-XRD patterns showed that Th-enriched (Fe-depleted) bauxite consists mostly of diaspore (AlOOH polymorph), anatase and rutile (TiO_2 polymorphs). SEM-EDS indicated the presence of Ti–Fe–containing phases (e.g. ilmenite, $FeTiO_3$), chromite (Cr-spinel) and besides LREE-minerals (mostly bastnäsite/parisite-group) and zircon ($ZrSiO_4$) hosting a part of the bulk Th. The presence of Th in diaspore and in Ti-containing phases (not detected by SEM-EDS as in the case of REE-minerals and zircon) was investigated, into distinct pisoliths of Fe-depleted bauxite, using μ-XRF and μ-XAFS in the SUL-X beamline of the ANKA Synchrotron facility (KIT, Germany). XAFS spectra of Th salts and Th-containing reference materials were obtained as well. Accordingly it was revealed, for the first time in the literature, that Ti-phases, and particularly anatase, host significant amounts of Th. This novel conclusion was complementary supported by LA-ICP-MS analyses indicated an average of 73 ppm Th in anatase grains together with abundant Nb (3356 ppm), Ta (247 ppm) and U (33 ppm). The Th L_{III}-edge XAFS spectra as compared to reference materials, give also evidence that Th^{4+} may not replace Ti^{4+} in distorted [TiO_6] fundamental octahedral units of anatase and ilmenite lattice (CN = 6). The occupation of either extraframework sites of higher coordination (CN = 6.9 or even CN = 7.4), according to EXAFS signals evaluation, or of defected/vacant (**) sites is more probable. This is likely explained by the difficulty of Th^{4+} to replace directly Ti^{4+} in [6]-coordinated (octahedral) sites due to the large difference in the relevant ionic radii (0.940 and 0.605 Å respectively).
© 2011 Elsevier B.V. All rights reserved.

1. Introduction

Greece is the 11th largest bauxite mine producer in the world (2.1×10^6 tons in 2009) and 1st in EU [1]. The exploitation of karst-type deposits in Parnassos-Ghiona area, central Greece e.g. [2,3], is currently performed by three Greek mining companies (Aluminium of Greece S.A., S&B Industrial Minerals S.A. and ELMIN Hellenic Mining Enterprises S.A.) whereas there is also an Al industrial plant in Corinth gulf. The mineralogy of Greek bauxite is not particularly variable. Diaspore and/or boehmite (AlOOH polymorphs), hematite (Fe_2O_3) and anatase and/or rutile (TiO_2 polymorphs) are the major phases. The accessory minerals include ilmenite ($FeTiO_3$), chromite (Cr-spinel), zircon ($ZrSiO_4$) and various REE-phases. Representative samples of typical Greek industrial bauxite, which is Fe-rich and red–brown in color, were found to contain an average of 57 wt.% Al_2O_3. High-quality (80 wt.% Al_2O_3) Fe-depleted or "bleached" (white–grey) bauxite is composed mainly of diaspore (in some cases Fe–Cr–diaspore [4]) and TiO_2 polymorphs (anatase and/or rutile). The entire chemical composition of bauxite is rather complicated and, except major Al, Fe and Ti, almost all natural elements are present in various concentrations including natural actinides (U and particularly Th). The

* Corresponding author. Tel.: +30 2107274689.
E-mail address: agodel@geol.uoa.gr (A. Godelitsas).

0168-583X/$ - see front matter © 2011 Elsevier B.V. All rights reserved.
doi:10.1016/j.nimb.2011.04.061

Author's personal copy

presence of Th in Greek karst-type bauxite is already known from few previous studies containing, however, only bulk analytical data [5–9]. Despite the fact that Th could be penalty element in the metallurgy and radiotoxic for the environment, relevant papers regarding Th partitioning (element distribution among the mineral phases) in bauxite from Greece or any other place of the world, are still absent. Consequently, the aim of the present study was to give new insights, for the first time in the literature, into the partitioning of Th in Greek industrial bauxite by combining diffraction (XRD), bulk analytical (XRF, ICP-MS, γ-ray spectroscopy), microscopic (SEM-EDS), and microscale-sensitive advanced spectroscopic techniques (Synchrotron μ-XRF and -XAFS as well as laser-ablation-ICP-MS). It should be emphasized that Synchrotron- and laser-based techniques have never been applied for the study of Greek bauxites whereas, as far as we know, there is only one previous work with XAFS spectra with regard to Zr in non-karst type bauxite [10].

2. Experimental

The investigated bauxite samples were obtained from underground active mining sites of the three Greek mining companies exploiting Al ores in the Parnassos-Ghiona area (central Greece). Bulk mineralogical composition was determined using powder X-ray diffraction/XRD (Bruker AXS D8 ADVANCE diffractometer, CuK_α radiation, 8 s per 2θ step with a step of 0.02°). Bulk chemical analyses were performed using X-ray Fluorescence/XRF (Philips MagiX Pro XRF with Rh Anode at 3.6 kW) and Inductively Coupled Plasma Mass Spectrometry/ICP-MS (Perkin–Elmer Sciex Elan 9000 ICP-MS following a $LiBO_2/LiB_4O_7$ fusion and HNO_3 digestion of a 0.2 g sample). Loss on ignition (LOI) was determined gravimetrically by heating the samples to 1000 °C. Gamma-ray spectra, towards the determination of radioactivity due to Th (^{228}Ac from ^{232}Th-series) were performed using a Canberra system with HPGe detector. Details on the mineralogical composition were obtained using SEM-EDS (Jeol JSM-5600 equipped with an Oxford Instruments INCA EDS). The sample chosen for further study using advanced spectroscopic techniques concerned Fe-depleted (white–grey) bauxite containing, according to previous measurements the highest Th concentration and the simplest mineralogical composition. Synchrotron radiation (SR) micro-X-ray Fluorescence (μ-XRF) and micro X-ray Absorption Fine Structure (μ-XAFS) spectra were obtained using powders and polished sections (Fig. 1) in the X-ray beamline of the Laboratory for Environmental Studies (SUL-X) of ANKA facility (KIT, Germany) e.g. [11]. Thorium compounds ($Th(NO_3)_4{\cdot}4H_2O$ and ThO_2) and minerals containing Th impurities, such as zircon ($ZrSiO_4$), were used as reference materials. Spectra were measured at the Th L_{III}-edge (16,300 eV) and processing was performed using initially the Athena [12] and furthermore the EDA [13] software packages. The EXAFS signal corresponding to the first main peak in Fourier transforms (FTs) was isolated using the Fourier filtering procedure. The range of the back-FT was 1–3 Å for $Th(NO_3)_4{\cdot}4H_2O$ and 0.8–2.5 Å for other samples. Thus, obtained EXAFS signals were best-fitted using two different approaches, namely, the conventional Gaussian model and the regularization method [14]. The theoretical backscattering amplitude and phase shift functions for Th–O were used in the simulations. They were calculated by the ab initio FEFF8 code [15] using a complex Hedin-Lundqvist exchange–correlation potential accounting for inelastic effects. Distinct mineral phases hosting Th, according to SR μ-XRF, were also point analyzed for trace element distribution by means of Laser Ablation Inductively Coupled Plasma Mass Spectrometry/LA-ICP-MS at WWU Münster, Germany [16]. Sample ablation for trace elements analysis has been done with a 193 nm ArF excimer laser (UP193HE, New Wave Research). The energy density was ~9 J/cm^2 and the laser repetition rate was set to 5 Hz. Depending on the size of the distinct mineral phases the beam spot diameter was varied from 12 to 25 μm. Elemental analysis has been carried out with an Element 2 mass spectrometer (ThermoFisher). Gas-flow rates were 0.73 l/min for

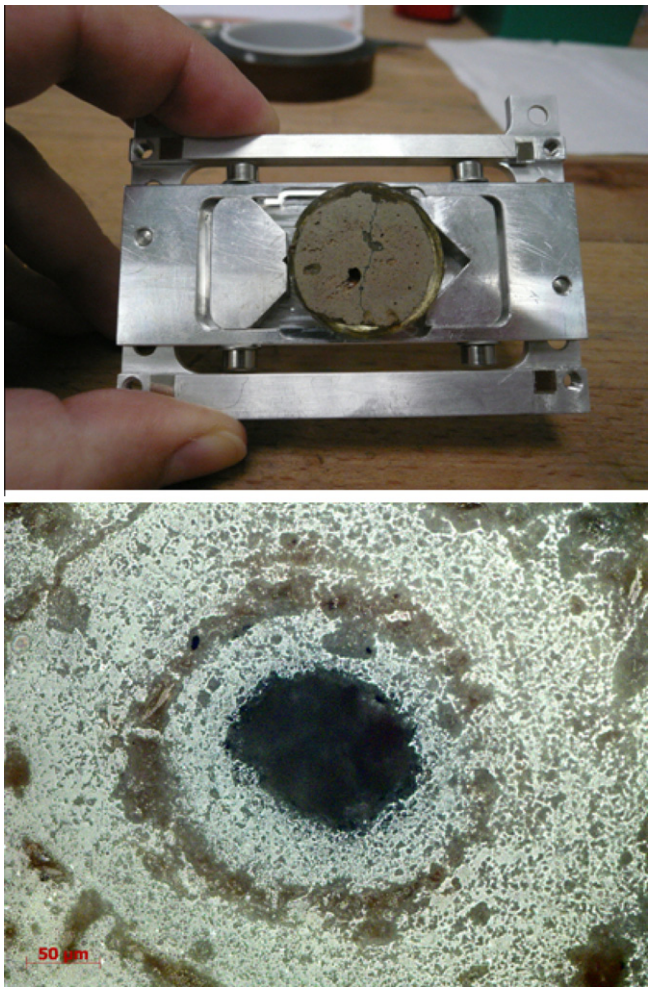

Fig. 1. Polished-section of Fe-depleted diasporic Greek industrial bauxite sample (upper) and detail of pisolith in the optical microscope (lower) prior to the μ-XRF and μ-XAFS measurements in the SUL-X beamline of ANKA.

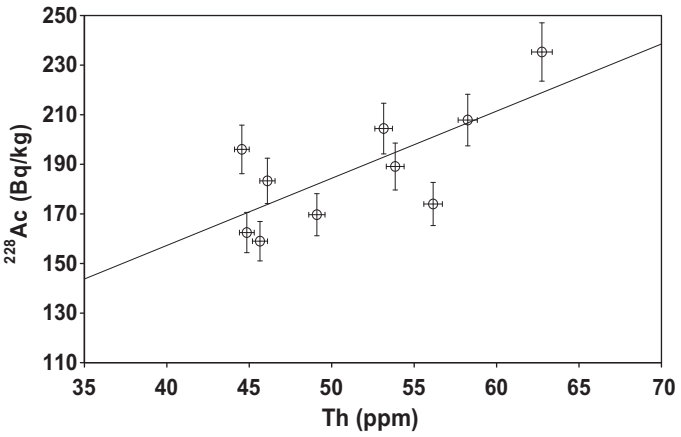

Fig. 2. Correlation of Th-induced radioactivity, due to ^{228}Ac (^{232}Th-series isotopes), with bulk content of Th in all types of Greek industrial bauxites.

Author's personal copy

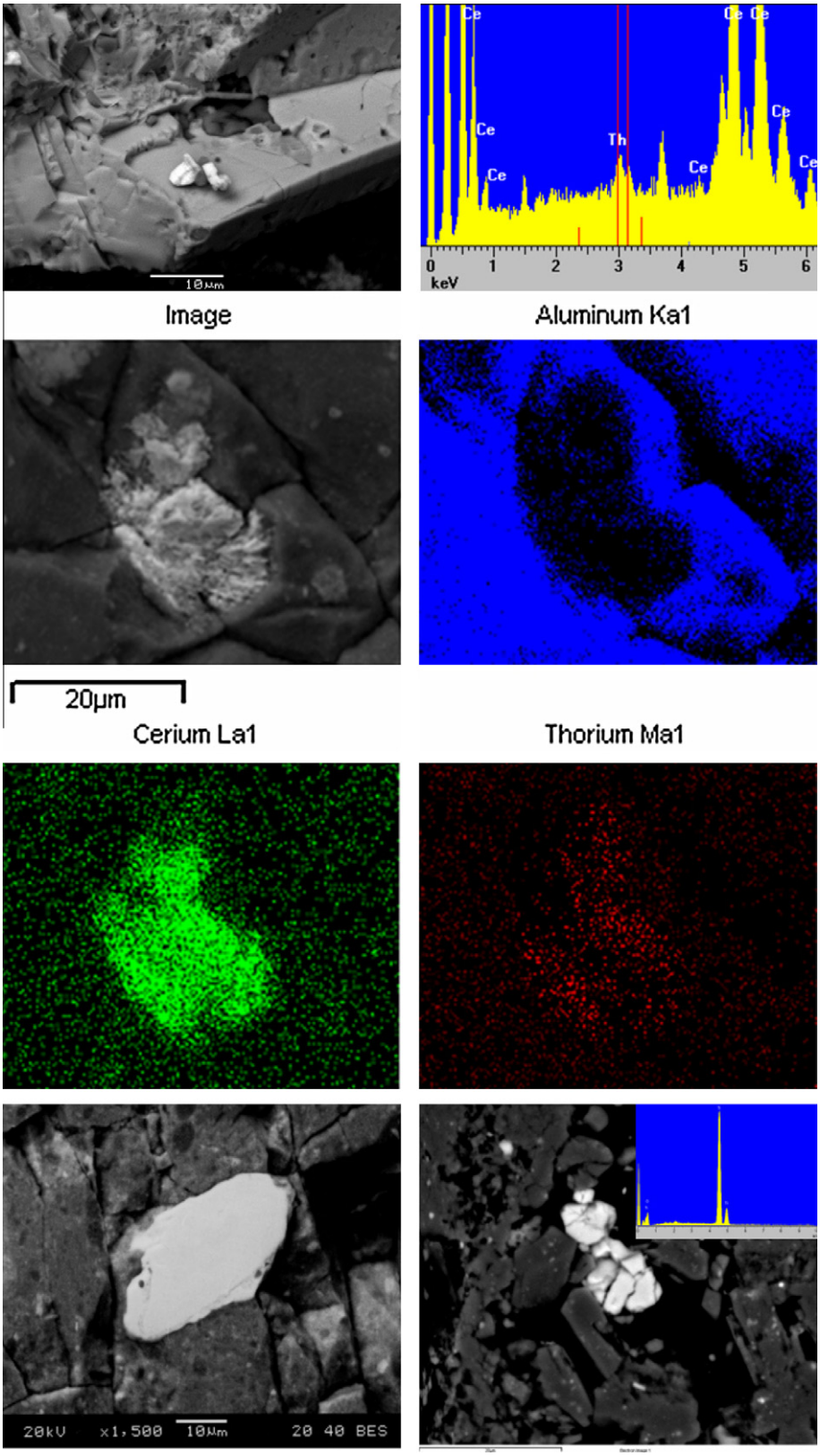

Fig. 3. SEM image and EDS spectrum of REE-phase deposited into a cavity of diasporic bauxite (upper). SEM image and EDS elemental maps of Th-containing REE fluorocarbonate mineral grown in the diasporic matrix of bauxite. (middle). Zircon crystal and anatase grain (the EDS spectrum indicating only Ti and not any Th is also included) into diasporic bauxite (lower).

the He carrier gas, 0.99 and 1 l/min for the Ar-auxiliary and sample gas, respectively. Cooling gas flow rate was set to 16 l/min. Before starting measurements, the system has been tuned on the SRM 612 standard glass from NIST to ensure high sensitivity and stability of the signal. A total of five (5) elements were analyzed using the NIST 612 glass as an external standard, and ^{49}Ti as internal standard.

Author's personal copy

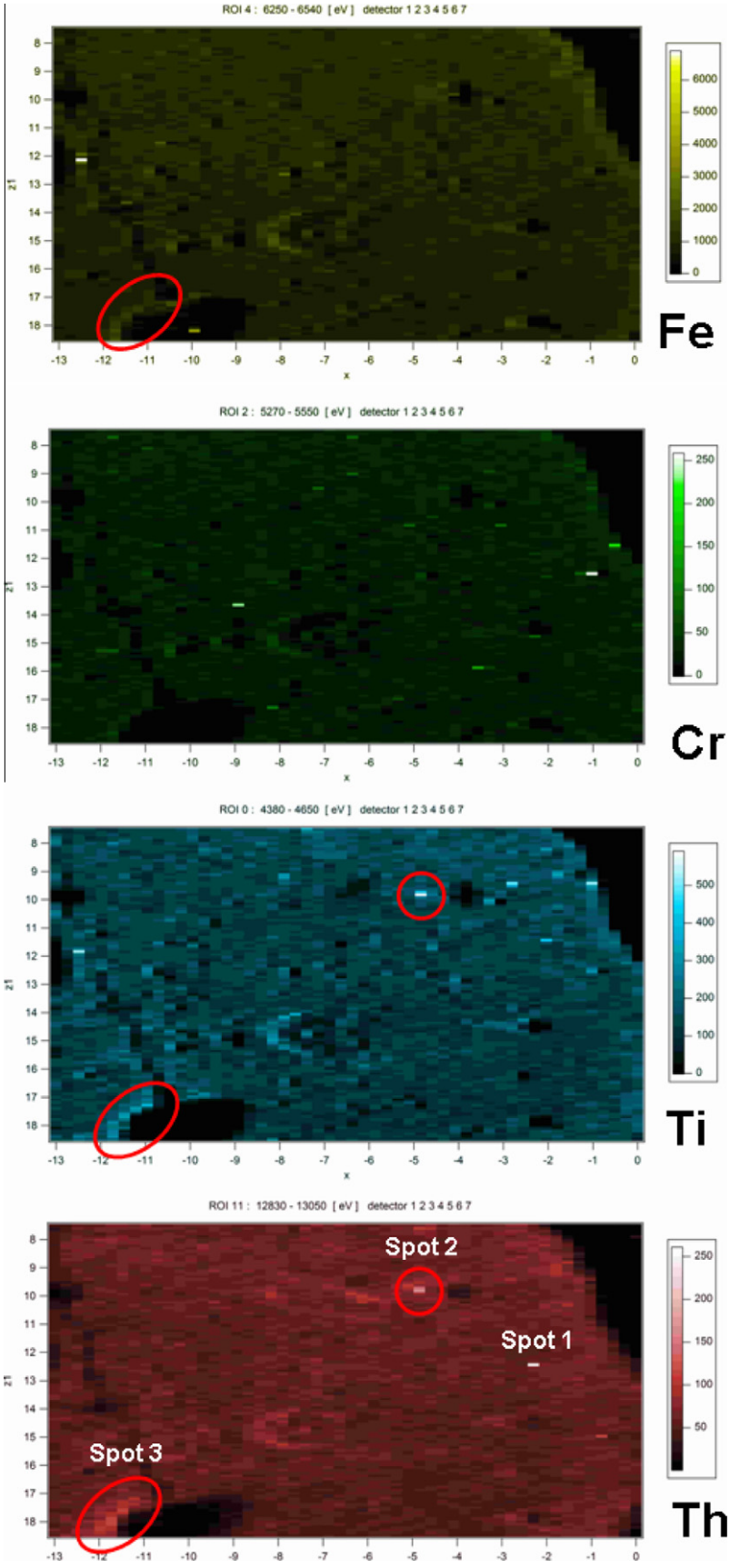

Fig. 4. Synchrotron μ-XRF elemental maps of Fe-depleted diasporic Greek industrial bauxite indicating the regions (Spot 2 & Spot 3) where μ-XAFS spectra were obtained.

Groups of five (5) spots on a given sample were bracketed with 2 calibration standards on both sides, to follow instrumental drift. The overall measuring time for a single spot analysis was 60 s (20 s for background and 40 s for the peak signal). Concentrations

Author's personal copy

Table 1
LA-ICP-MS analyses of selected anatase (TiO_2) crystals from Fe-depleted or "bleached" industrial bauxite from Parnassos-Ghiona mining area, Greece (sample code: ALM0306_PL1_BIW); units in ppm.

	Nb	Ta	Th	U
TiO_2 #1	1759	55	28	6
Error (1 sigma)	153	4	2	1
TiO_2 #2	1913	64	61	13
Error (1 sigma)	178	5	5	1
TiO_2 #3	2278	82	104	20
Error (1 sigma)	229	7	9	2
TiO_2 #4	1443	54	13	7
Error (1 sigma)	156	5	1	1
TiO_2 #5	947	77	106	97
Error (1 sigma)	129	9	12	13
TiO_2 #6	3286	414	117	69
Error (1 sigma)	481	53	14	10
TiO_2 #7	11,865	982	82	17
Error (1 sigma)	1857	135	11	3

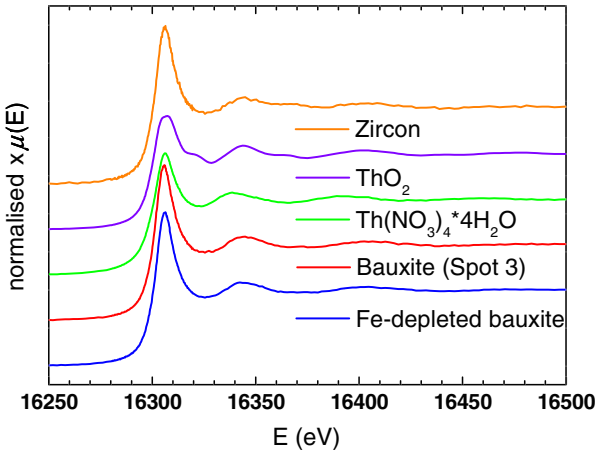

Fig. 5. Th L_{III}-edge XAFS spectrum (bulk) of Fe-depleted diasporic Greek industrial bauxite (processing using the Athena software [12]), together with μ-XAFS spectrum from Spot 3, in comparison with spectra of reference materials: $Th(NO_3)_4{\cdot}4H_2O$, ThO_2 and zircon ($ZrSiO_4$).

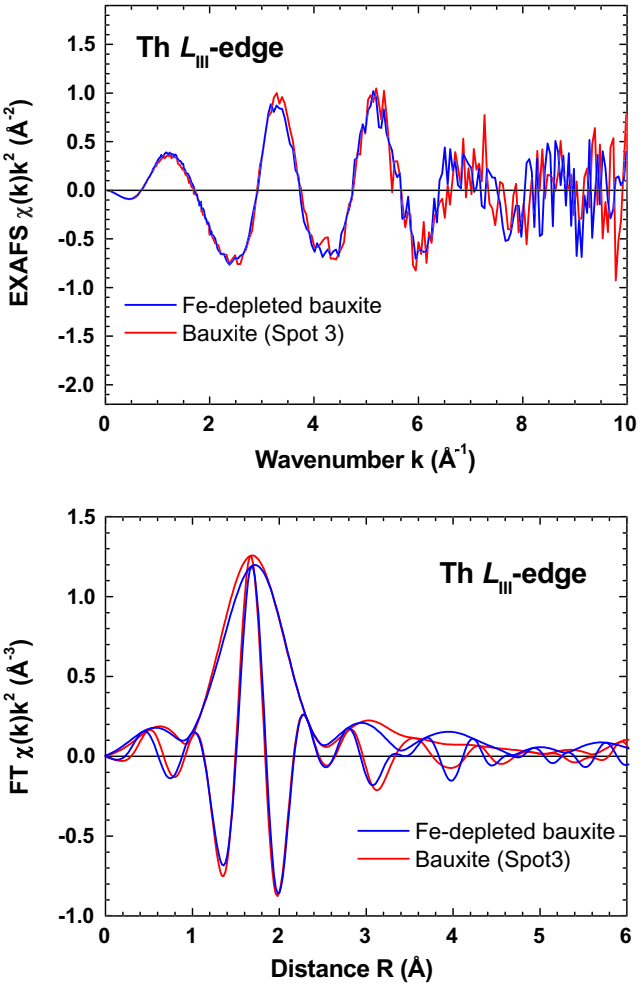

Fig. 6. Experimental Th L_{III}-edge EXAFS signals (upper) and their Fourier transform (lower) using the EDA software package [13].

of measured elements were calculated using the Glitter software [17].

3. Results and discussion

The XRD of all investigated bauxite samples proved as major phases AlOOH polymorphs (diaspore and/or boehmite), Fe-oxides (hematite and/or magnetite) and TiO_2 polymorphs (anatase and/or rutile) as well as, occasionally, Fe-oxyhydroxides (goethite) and clays (kaolinite). The Th-rich Fe-depleted bauxite, subjected to further Synchrotron- and laser-based study, was found to contain only diaspore and anatase with minor rutile. The bulk analyses for Th obtained by XRF are in good agreement with those obtained by ICP-MS ($R^2 = 0.94$, $n = 17$). The Fe-rich samples show an average of ca. 49 ppm whereas the Fe-depleted samples ca. 40 ppm, in agreement with the bulk Th ranges in previous works [5–9]. However, the highest bulk Th concentration (62.75 ppm in bulk) corresponds to the specific diasporic Fe-depleted sample studied by advanced spectroscopic techniques. Evaluation of the bulk geochemical data (taking into account more trace elements analyzed by XRF and ICP-MS) indicated that Th is correlated to LREE (e.g. La, Ce) and U, particularly in Fe-depleted bauxite. Moreover, Th is rather correlated to Fe in Fe-rich bauxite, while there is no evident bulk correlation to Ti for all bauxite samples. Furthermore, γ-ray measurements, correlated to Th bulk concentrations (Fig. 2), revealed an average activity of 220 Bq/kg corresponding to ^{228}Ac (^{232}Th-series) for Fe-depleted bauxite (max. 235 Bq/kg) compared to an average of 180 Bq/kg for Fe-rich bauxite. The total average, for all types of Greek bauxite examined, is 188 Bq/kg ($n = 10$), in general agreement with data from a previous investigation (216 Bq/kg, $n = 2$) [18]. This value is lower than the average of Hungarian bauxite (256 Bq/kg, $n = 46$) and much lower than the international average (400 Bq/kg) [19]. The SEM-EDS investigation, aiming to detection of Th-containing minerals prior to Synchrotron and LA-ICP-MS studies revealed the significant concentrations of the actinide element in LREE-minerals (mostly bastnäsite/parisite-group [20,21] with up to 2.5 wt.% ThO_2) as well as to zircon ($ZrSiO_4$) detrital crystals (Fig. 3). Previous microscopic studies about REE-phases in Greek bauxites have not reported the presence of Th [22], while Th-containing Y-phosphates [23] have not been approved, in spite careful SEM-EDS, in the frame of the present study. It is noteworthy that the obtained SEM-EDS results concerning the existence of Th in LREE-minerals in Greek bauxites are presented for the first time in the literature. It should also be emphasized that Th was not detected in AlOOH matrix or in any other Fe-, Ti- and Fe–Ti-phase (Fig. 3).

The SR μ-XRF elemental maps, supplying direct evidence that Th is associated with Ti- and Fe/Ti-containing phases into distinct pisoliths of Fe-depleted bauxite, are presented in Fig. 4. These phases, according to the present XRD and SEM-EDS data and taking into account the data about Ti-phases in karst-type bauxites of the world [2,24], should be anatase and/or rutile and ilmenite. Based

Author's personal copy

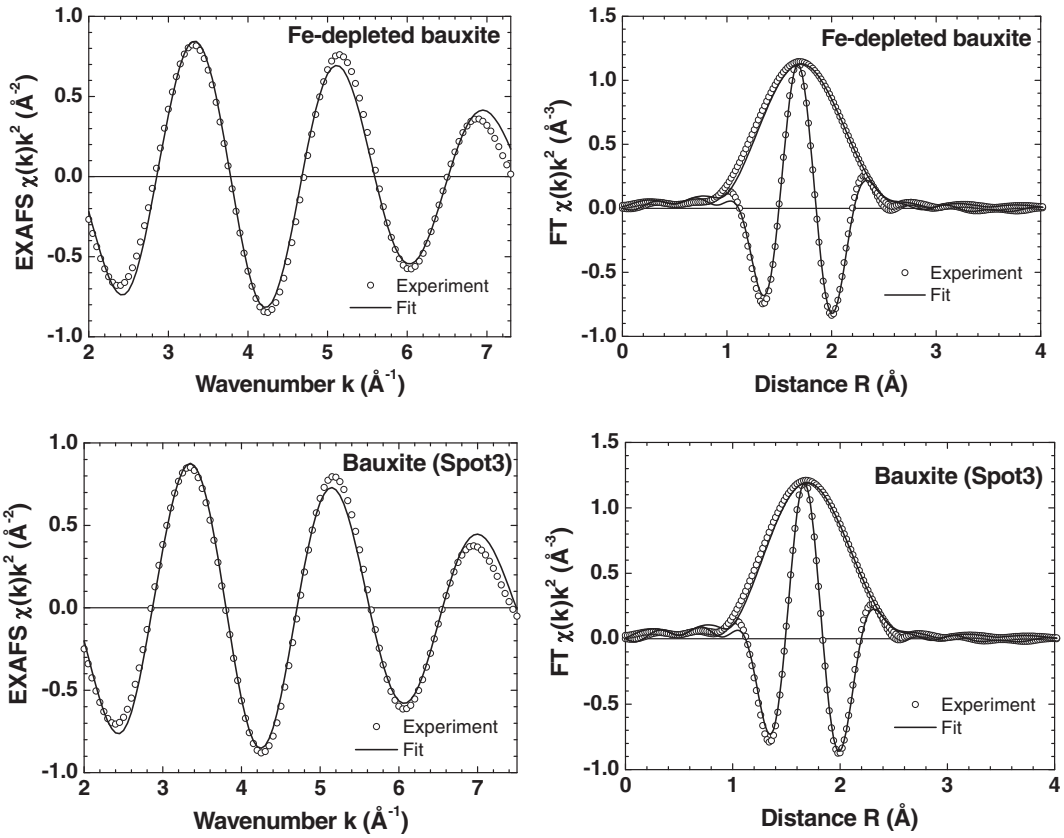

Fig. 7. First shell EXAFS fit using single-shell Gaussian model.

on previous preliminary data about the nature of TiO_2 phases in Greek Fe-depleted bauxite [4], the Th-containing TiO_2 phases must be anatase while rutile crystals are much smaller and almost below the resolution of the beamline. Our data are in line with previous bulk [25,26], SR μ-XRF [27,28], and LA-ICP-MS [29,30] studies with regard to Th in synthetic and natural TiO_2 phases (rutile) as well as ilmenite occurring in geological materials other than bauxite (e.g. black sands). The μ-XRF data about Th partitioning in Fe-depleted bauxite were complementary checked by applying LA-ICP-MS on seven selected anatase grains (up to 20 μm, see also Fig. 3). The results shown in Table 1 confirmed that Th concentration varies in the range of 13–117 ppm together with abundant Nb (947–11,865 ppm), Ta (55–982 ppm) and U (6–97 ppm). It is therefore demonstrated that Th is associated with Ti- and Fe/Ti-containing phases in microscale despite the fact that bulk analyses indicated no correlation of Th to Ti (effect of "scale-factor" [31]).

The recorded Th L_{III}-edge XAFS spectra of Fe-depleted (white–grey) bauxite and reference materials, as powders, together with μ-XAFS spectra from Spot 3 (see Fig. 4), are presented in Fig. 5. The Th L_{III}-edge XAFS spectra of bauxite (bulk and in microscale) show a shift towards higher energy in the first EXAFS oscillation as compared to $Th(NO_3)_4{\cdot}4H_2O$ possessing 12-coordinated Th ions [32]. This indicates, according to methodology of Harfouche et al. [33], who studied the coordination of Zr^{4+} to zircon using Zr $L_{II/III}$-edge XANES spectra, that Th most possibly undergoes to a coordination number lower than twelve (CN < 12). At the same time there is a higher similarity to ThO_2 hosting 8-coordinated Th-ions e.g. [34]. That means, Th in bauxite most likely reduces to a coordination number close to eight (CN ≈ 8), i.e. higher than six (CN > 6), as well. The above data show that Th^{4+} ions do not replace 6-coordinated Ti^{4+} ions in distorted [TiO_6] fundamental octahedral units (framework) of anatase [35] and ilmenite lattice. It is known that Th is incorporated as impurity (from 0.5 to >5000 ppm, e.g. [36]) in natural zircon together with several other trace elements (such as Hf, Y, P, U and REE, e.g. [36,37]). According to Muñoz et al. [38] Zr ↔ Th substitution is possible because thorite ($ThSiO_4$) and zircon are isostructural ($I4_1/amd$). Additionally, Harfouche and Farges have mentioned, in a recent report [39], a local expansion around actinides substituting for Zr, which is a function of the metamictisation degree. Thus, zircon hosts 8-coordinated Th ions in radiation-undamaged structure whereas their coordination drops to seven in the damaged structures. The similarity of Th L_{III}-edge XAFS spectra of bauxite to that of reference zircon (Fig. 5), as well as to ThO_2, indicates that Th ions (predominantly contained in anatase) are coordinated by about 7–8 oxygen atoms and therefore the coordination number is seven or eight (CN = 7 or 8). This is supported by the evaluation of the EXAFS signals (Fig. 6). The best-fits of the first peak contribution by one-component Gaussian model are shown in Fig. 7. As one can see, the agreement is acceptable, though a short k-space range strongly limits the resolution in R-space and also makes the values of coordination numbers –CN– to be strongly correlated with that of Debye–Waller factors σ^2. In this case, the use of two models resulted in slightly different Radial Distribution Functions – RDFs – (Fig. 8). The observed difference is due to the asymmetric shape of the RDF which cannot be reproduced by the Gaussian model (Table 2).

The coordination number value, which is between seven and eight (CN = 7.4 as revealed by regularization method), strongly supports the statement that Th^{4+} does not replace Ti^{4+} (CN = 6) in anatase, and even ilmenite, framework. The formation of Th-polyhedra (perhaps distorted) by occupation of either extraframework sites or of defected/vacant (□) sites is more probable. This is likely explained by the difficulty of Th^{4+} to replace directly Ti^{4+} in [6]-coordinated (octahedral) sites due to the large difference in the relevant ionic radii (0.940 and 0.605 Å, respectively [40]). The above results give new aspects into mineral-chemistry of Th in karst-type

Author's personal copy

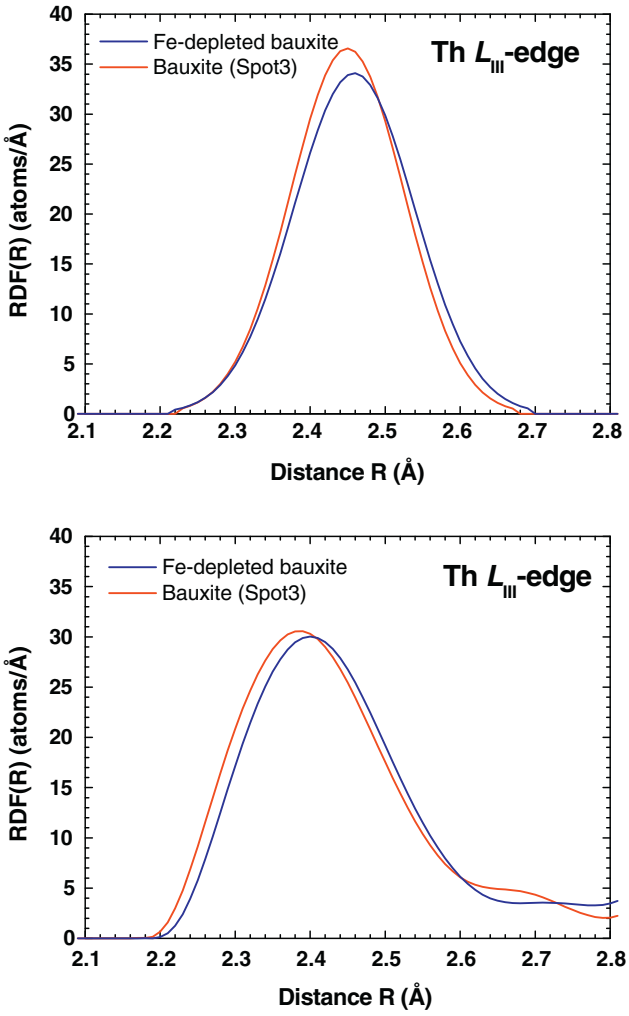

Fig. 8. Radial Distribution Function – RDF – using conventional Gaussian model (upper) and regularization method [14] (lower).

Table 2
Structural parameters obtained from the processing of the EXAFS signals using the EDA software package [13].

	Fe-depleted bauxite	Spot 3
Gaussian model		
CN ± 0.7	6.9	6.9
R (Å) ± 0.04	2.46	2.45
σ^2 (Å^2) ± 0.002	0.007	0.006
Regularization method		
CN	7.4	7.4
R (Å)[a]	2.40	2.38

[a] This distance is the position of the RDF maximum.

bauxite and reveal the geochemical mechanisms allowing Ti- and Ti–Fe oxides, that deposited into cavities on karstic surfaces of carbonate platforms at low-temperature environments, together with insoluble chemical compounds (mostly Al-oxyhydroxides), to control the immobilization of dissolved Th ions.

Acknowledgements

Aluminium of Greece S.A., S&B Industrial Minerals S.A. and ELMIN Hellenic Mining Enterprises S.A. are gratefully acknowledged for provision of bauxite samples from active mines of Parnassos-Ghiona area and collaboration in P.G.'s PhD Thesis. We would also like to thank Dr. Burkhard Schulz-Dobrick (Johannes Gutenberg University, Mainz) for collaboration in XRF analysis. Finally, we acknowledge the Synchrotron Light Source ANKA for provision of beamtime at the SUL-X beamline.

References

[1] US Geological Survey, Mineral Commodity Summaries 2011, USGS, Reston, Virginia, 2011, p. 198..
[2] G. Bárdossy, Karst Bauxites – Bauxite Deposits on Carbonate Rocks, Elsevier, Amsterdam, 1982. p. 441.
[3] I. Valeton, M. Biermann, R. Reche, F. Rosenberg, Ore Geol. Rev. 2 (1987) 359.
[4] P. Gamaletsos, A. Godelitsas, A.P. Douvalis, T. Kasama, R.E. Dunin-Borkowski, J. Göttlicher, N. Church, G. Economou, T. Bakas, Geochim. Cosmochim. Acta 73 (2009) A409.
[5] J.A.S. Adams, K.A. Richardson, Econ. Geol. 55 (1960) 1653.
[6] S. Papastavrou, V. Perdikatsis, in: S. Janković (Ed.), Mineral Deposits of the Tethyan Eurasian Metallogenic Belt between the Alps and the Pamirs, UNESCO/IGCP Project No 169, Faculty of Mining and Geology, Belgrade University, 1987, p. 111.
[7] K.M. Ochsenkühn, M. Ochsenkühn-Petropoulou, G. Parissakis, J. Radioanal. Nucl. Ch. 190 (1) (1995) 75.
[8] K.M. Ochsenkühn, P. Fafouteli, M. Ochsenkühn-Petropoulou, J. Radioanal. Nucl. Ch. 253 (2) (2002) 257.
[9] M. Laskou, M. Economou-Eliopoulos, J. Geochem. Explor. 93 (2007) 67.
[10] L. Duvallet, F. Martin, F. Soubiès, S. Salvi, A.J. Melfi, J.P. Fortuné, Can. Mineral. 37 (1999) 635.
[11] J. Göttlicher, R. Steininger, R. Simon, 12th European Conf. On X-Ray Spectroscopy (EXRS 2006), Paris, F, June 19–23, 2006.
[12] B. Ravel, M. Newville, J. Synchrotron. Radiat. 12 (2005) 537.
[13] A. Kuzmin, Phys. B 208–209 (1995) 175.
[14] A. Kuzmin, J. Purans, J. Phys.: Condens. Matter 12 (2000) 1959.
[15] A.L. Ankudinov, B. Ravel, J.J. Rehr, S.D. Conradson, Phys. Rev. B 58 (1998) 7565.
[16] A.K. Engvik, U. Golla-Schindler, J. Berndt, H. Austrheim, A. Putnis, Lithos 112 (2009) 236.
[17] S.E. Jackson, Mineral. Assoc. Can. Short Course Ser. 29 (2001) 29.
[18] G. Papatheodorou, H. Papaefthymiou, A. Maratou, G. Ferentinos, Radioprotection 40 (2005) 549.
[19] J. Somlai, V. Jobbágy, J. Kovács, S. Tarján, T. Kovás, J. Hazard. Mater. 150 (2008) 541.
[20] J.D. Grice, V. Maisonneuve, M. Leblanc, Chem. Rev. 107 (2007) 114.
[21] Z.J. Maksimović, Gy. Pantó, in: A.P. Jones, F. Wall, C.T. Williams (Eds.), Rare Earth Minerals, Chapman & Hill, London, 1996, p. 372.
[22] M. Ochsenkühn-Petropoulou, K.M. Ochsenkühn, Eur. Microscos. Anal. (1995) 13.
[23] M. Laskou, G. Andreou, in: Eliopoulos, D., et al., Mineral Exploration and Sustainable Development, 7th Biennial SGA Meeting, Athens, Millpress, Rotterdam, 2003, p. 89.
[24] I. Valeton, Bauxites – Developments in Soil Science 1, Elsevier, Amsterdam, 1972. p. 226.
[25] A. Filippidis, P. Misaelides, A. Clouvas, A. Godelitsas, N. Barbayiannis, I. Anousis, Environ. Geochem. Hlth. 19 (1997) 83.
[26] P.P. Haridasan, P.M.B. Pillai, R.M. Tripathi, V.D. Puranik, Radiat. Prot. Dosim. 129 (4) (2008) 381.
[27] R.F. Garrett, N. Blagojevic, Z. Cai, B. Lai, D.G. Legnini, W. Rodrigues, A.P.J. Stampfl, Nucl. Instrum. Methods A 467–468 (2001) 897.
[28] P. Kappen, J.V. Dubrawski, P.J. Pigram, in HASYLAB Annual Report 2007.
[29] T. Zack, A. Kronz, S.F. Foley, T. Rivers, Chem. Geol. 184 (2002) 97.
[30] S. Klemme, S. Prowatke, K. Hametner, D. Günther, Geochem. Cosmochem., Acta 69 (9) (2005) 2361.
[31] G. Bárdossy, in: G. Maros (Ed.), The Halimba bauxite deposit, Geological Institute of Hungary, 2007, p. 119.
[32] P.P. Charpin, G. Chevrier, M. Lance, M. Nierlich, N.D. Vigner, J. Livet, C. Musikas, Acta Cryst. C43 (1987) 1239.
[33] M. Harfouche, F. Farges, J.P. Crocombette, A.M. Flank, Phys. Scripta T115 (2005) 928.
[34] M.O. Figueiredo, J. Mirão, Eur. J. Mineral. 14 (2002) 1061.
[35] M. Horn, C.F. Schwerdtfeger, E.P. Meagher, Z. Kristallogr, Z. Kristallogr. 136 (1972) 273.
[36] U. Poller, J. Huth, P. Hoppe, I.S. Williams, Am. J. Sci. 301 (2001) 858.
[37] C.B. Grimes, B.E. John, P.B. Kelemen, F.K. Mazdab, J.L. Wooden, M.J. Cheadle, K. Hanghøj, J.J. Schwartz, Geology 35 (2007) 643.
[38] M. Muñoz, P. Argoul, F. Farges, Am. Mineral. 88 (2003) 694.
[39] M. Harfouche and F. Farges, 25th European Crystallographic Meeting, ECM 25, Instanbul, 2009, Acta Cryst. A65 (2009), s118.
[40] R.D. Shannon, Acta Cryst. A32 (1976) 751.